Available online at www.sciencedirect.com
SCIENCE DIRECT®
Journal of Sound and Vibration 285 (2005) 73–99
JOURNAL OF SOUND AND VIBRATION
www.elsevier.com/locate/jsvi

Study on the influence of friction in an automatic ball balancing system

Quangang Yang[a,*], Eng-Hong Ong[a], Jisong Sun[a], Guoxiao Guo[a], Siak-Piang Lim[b]

[a]*Data Storage Institute, 5 Engineering Drive 1, Singapore 117608, Singapore*
[b]*Department of Mechanical Engineering, National University of Singapore, 10 Kent Ridge Crescent, Singapore 119260, Singapore*

Received 25 July 2003; received in revised form 13 July 2004; accepted 11 August 2004
Available online 15 December 2004

Abstract

This study aims to investigate the influence of friction in an automatic ball balancing system. A precise kinetic model is presented for a commercial optical disk drive with an automatic ball balancer. The equations of motion, with the effects of frictional and driving forces taken into account, are derived based on this model. To investigate the influence of friction on the dynamic behavior of the system, different friction coefficients and initial ball positions were considered and the equations were solved numerically with a commercial software package, Matlab. The results do not only indicate that friction prevents the ball from reaching the desired positions to automatically balance the system but also reveal that the balls can be set into oscillation in steady state. Finally, experiments are designed and carried out to verify the theoretical analysis.

1. Introduction

The imbalance in various rotating machines, ranging from small size computer hard disk drives (HDDs) to large size gas turbines, generates undesirable centrifugal force and induces vibrations, compromising the performance and efficiency of the system and eventually causes damage to it. The automatic ball balancer (ABB) has been increasingly studied recently to facilitate the

*Corresponding author.
E-mail address: qg_yang@hotmail.com (Q. Yang).

0022-460X/$ - see front matter © 2004 Elsevier Ltd. All rights reserved.
doi:10.1016/j.jsv.2004.08.009

balancing of a rotating machine during its operation [1–8]. This approach has already been applied to many systems ranging from CD-ROM to washing machines. Also, many patents have been granted to the various ABBs proposed.

In its simplest form, an ABB comprises a circular disk or ring with a groove that contains balls free to move in it. The current difficulties in the design and application of ABB to a system that can only tolerate ultra low imbalance are associated with the lack of an accurate model that takes friction between the balls and the groove into account. The early research carried out by Bövik and Högfors [1] showed the auto balancing effects of an ABB for both planar and non-planar rotors. Recently, Chung and Ro [3] have analyzed in detail the stability and dynamic behavior of an automatic balancing system. They investigated influences of the different parameters, such as rotational speed, mass ratio and internal and external dampings, on the system stability. Using the same method, Chung and Jang [4] also studied the stability and time responses of an ABB supported by a single flexible shaft with the gyro effects taken into account. In their papers, the time responses were computed by employing the generalized-α method; however, the influence of friction was not taken into consideration. Kim and Chung [5] presented a dynamic model for an ABB fitted on an optical disk drive. Both the translational and rotational displacements of the feeding deck were considered in the equations of motion, and they use the Floquet theory in analyzing the stability because it is a non-autonomous system. Rajalingham et al. [6,7] proposed a model to analyze the stability of a single-ball balancing system using a rotating reference frame. Although both the external and internal dampings of the system were not considered in their model, friction was first considered indirectly and was thought to be proportional to the ball's angular acceleration [7]. The effects of friction were also studied indirectly by Huang et al. [8]. They investigated the dynamics effects of runway eccentricity, rolling resistance and drag force on a rotor-balancer system in an optic disk drive in order to reduce its vibrations.

Frictional forces on the balancing balls play a very important role in determining whether they can reach their desired positions, especially for balls in a system without liquid filled in the racetrack, such as the one found in commercial CD-ROMs. In this paper, instead of dealing with the stability of an ABB, we focus on probing the influence of friction on the ABB's performance. A precise kinetic model is presented for a commercial optical disk drive with an ABB. After examining the vibration characteristics of an unbalanced rotating system, the forces acting on a balancing ball in steady state are formulated. The driving force on the ball is thus obtained, and the stable and unstable equilibrium positions are identified. And also, the condition to move a ball is ascertained by comparing the driving with frictional forces on it. The equations of motion, with the effects of frictional and driving forces taken into account, are then derived. The time responses are subsequently acquired by employing a commercial software package, Matlab. The results not only indicate the friction's influence on balls' final dwelling ranges around the desired positions and consequently, the performance of an ABB but also reveal the existence of oscillatory steady states. Finally, experiments are designed and carried out to verify the theoretical analysis.

2. Vibration characteristics of an unbalanced optical disk drive

Fig. 1 shows the interior of a commercial optical disk drive that comes with an ABB. The motor is rigidly fixed on a support plate which is mounted onto the base with four rubber washers. The

ABB is attached to the shaft extension of the spindle motor and the disk is then pressed on the ABB by a magnetic clamp. The ABB comprises an annular structure with a groove containing balls. The balancing balls are able to move in the racetrack freely and the motor rotates with an angular velocity of ω (or denoted as Ω in rpm).

All the parts, except suspension washers, are considered to be rigid. And also, the dynamics of the spindle motor bearing is neglected in the discussion because the bearing is much more stiffer than the suspension washers. The physical system can then be simplified as the model shown in Fig. 2, where G, C and O denote the gravity center, geometry center and whirling center, respectively, with CG being the eccentricity denoted by ε. As described in Ref. [9] for the Jeffcott

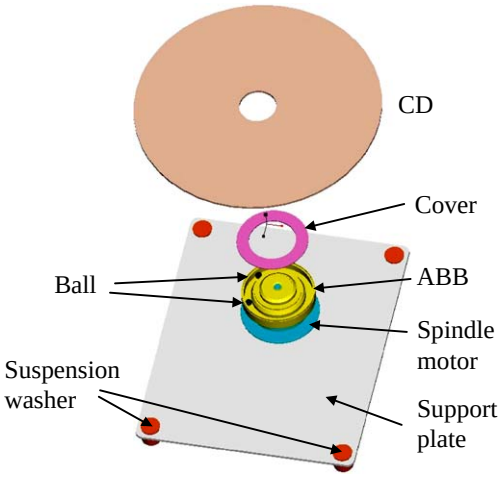

Fig. 1. An optical disk drive with ABB.

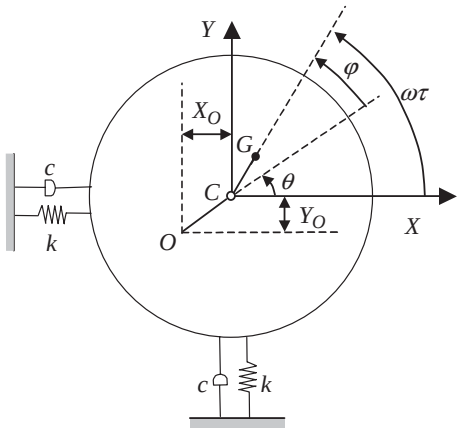

Fig. 2. Analytical model of the system.

rotor, the equations of motion can be written as

$$M\ddot{X}_O + c\dot{X}_O + kX_O = m\varepsilon\omega^2 \cos(\omega t), \tag{1}$$

$$M\ddot{Y}_O + c\dot{Y}_O + kY_O = m\varepsilon\omega^2 \sin(\omega t), \tag{2}$$

where M is the total mass, m is the mass of the rotating parts, and $m\varepsilon$ is the imbalance in unit of gram-meter.

Introducing the damping factor ζ and natural frequency ω_n, these two equations take the form

$$\ddot{X}_O + 2\xi\omega_n\dot{X}_O + \omega_n^2 X_O = \frac{m}{M}\,\varepsilon\omega^2 \cos(\omega t), \tag{3}$$

$$\ddot{Y}_O + 2\xi\omega_n\dot{Y}_O + \omega_n^2 Y_O = \frac{m}{M}\,\varepsilon\omega^2 \sin(\omega t). \tag{4}$$

The steady-state responses are then given by

$$X_O = \frac{m}{M}\,\frac{\varepsilon\varpi^2}{\sqrt{(1-\varpi^2)^2 + (2\zeta\varpi)^2}} \cos(\omega t - \varphi), \tag{5}$$

$$Y_O = \frac{m}{M}\,\frac{\varepsilon\varpi^2}{\sqrt{(1-\varpi^2)^2 + (2\zeta\varpi)^2}} \sin(\omega t - \varphi), \tag{6}$$

where

$$\varpi = \frac{\omega}{\omega_n}, \tag{7}$$

$$\varphi = \tan^{-1}\left(\frac{2\xi\varpi}{1-\varpi^2}\right). \tag{8}$$

Thus,

$$R_w = \sqrt{Y_O^2 + X_O^2} = \frac{m}{M}\,\varepsilon\,\frac{\varpi^2}{\sqrt{(1-\varpi^2)^2 + (2\zeta\varpi)^2}}, \tag{9}$$

where R_w is the whirling circle radius. It is proportional to the mass ratio (m/M), eccentricity and the magnification factor.

Let θ denotes the angle between OC and$X$; then, we have

$$\theta = \tan^{-1}\left(\frac{Y_O}{X_O}\right) = \omega t - \varphi. \tag{10}$$

It suggests that the line OC also rotates at angular velocity ω, but lags behind the line CG by φ. As we know, φ is dependent on ϖ; the relative position of OC to CG is then presented in Fig. 3 with respect to ϖ.

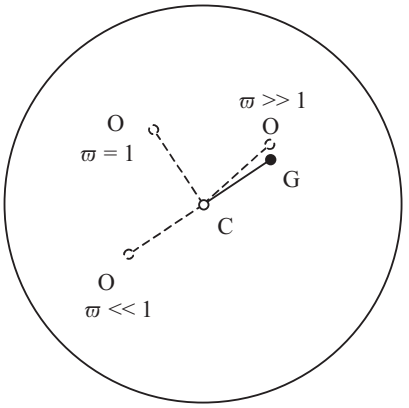

Fig. 3. Relative positions of OC and CG.

3. The forces acting on the balancing ball

As a ball balancing system approaches its steady state, the whirling radius reduces very much, and also, the ball's velocity in the racetrack gradually decreases to zero. However, the balls may not be able to reside at the desired positions exactly. Instead, they may stop at the vicinal points because the driving forces are not enough to overcome the frictional forces at these points. This will lead to the imbalance not compensated completely. The ball's dwelling range in steady state will be discussed through analysis of the forces acting on a still balancing ball at different locations in the racetrack shortly.

The forces acting on the balancing ball are indicated in Fig. 4. f_C is the centrifugal force caused by the system rotating around O. It can be decomposed into two components: f_r along the radial direction and f_t the tangential direction. The inertia forces in X and Y directions are ignored here, because they are very small in the steady state compared to the centrifugal force. f_t is actually the driving force on the ball; if it is larger than the frictional force, the ball moves. Let ϕ define the angular position of the ball at B with respect to the line CG, and then angle β from the ball to the line CO is expressed as

$$\beta = \phi + \varphi - \pi. \tag{11}$$

R_O is the distance from the ball to the whirling center O and it can be written as

$$R_O = \sqrt{R^2 + R_w^2 - 2RR_w \cos\beta}. \tag{12}$$

Hence, the centrifugal force f_C has the expression of

$$f_C = m_b\omega^2 R_O, \tag{13}$$

where m_b is the mass of balancing ball.

Thus, it can be shown that

$$f_t = f_C \sin\alpha = m_b\omega^2 R_w \sin\beta, \tag{14}$$

$$f_r = f_C \cos\alpha = m_b\omega^2(R - R_w \cos\beta). \tag{15}$$

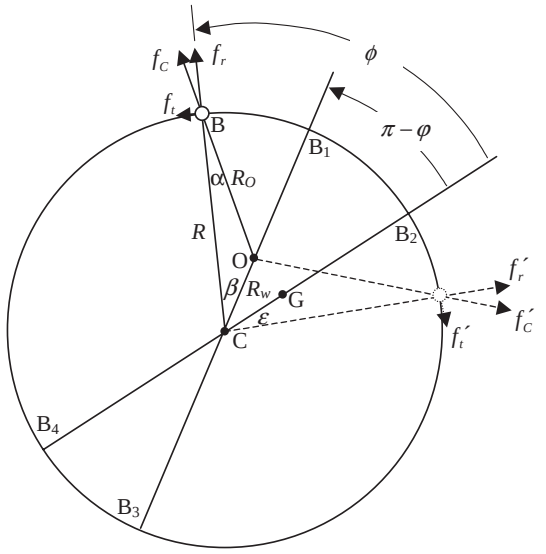

Fig. 4. Schematic diagram of forces acting on the ball.

For a ball located in the arc $B_1B_4B_3$, $\beta \in [0, \pi]$, f_t will be positive and the ball tends to move counter-clockwise, as indicated in Fig. 4. If a ball is located in the arc $B_1B_2B_3$, $\beta \in [-\pi, 0]$, f_t' is negative, indicating that the ball tends to move clockwise. Taking the gravity center G as the reference, it can be seen that if a ball is located in the arc B_1B_4 and B_2B_3, it is driven away from the imbalance. Outside these two arcs, the ball is directed to the imbalance. At B_1 and B_3, f_t will be zero, so that they can be considered as two equilibrium positions. However, for a ball at B_1, it moves away from this point once it gets a disturbance because on both sides of B_1 the ball's driving force directs it away from B_1. In contrast, a ball at B_3 goes back to B_3 after it is displaced from B_3 by a small disturbance, as the driving forces in the vicinal area make the ball move towards B_3. We therefore conclude that B_1 is an unstable equilibrium position and B_3 is a steady equilibrium position.

As indicated in the previous analysis, B_1B_3 is aligned with CO, the locations of B_1 and B_3 in the racetrack are hence dependent on ϖ. If $\omega \ll \omega_n$ ($\varpi \ll 1$), stable equilibrium B_3 will be very close to B_2, which is on the same side as the imbalance. Therefore, the imbalance of the system will increase rather than decrease, as the balancing balls will stay on the same side as the imbalance.

To move a ball located at an arbitrary position, the driving force f_t must be able to overcome the frictional force which is denoted as f_f. Hence, we arrive at the condition for the ball to move:

$$f_d = |f_t| - f_f = |f_t| - \mu f_r > 0. \tag{16}$$

Substituting Eqs. (14) and (15) into Eq. (16), and considering $\beta = \phi + \varphi - \pi$, leads to

$$f_d = m_b\omega^2[R_w|\sin(\phi+\varphi)| - \mu(R + R_w\cos(\phi+\varphi))] = m_b\omega^2 R', \tag{17}$$

where $R' = R_w[|\sin(\phi+\varphi)| - \mu\cos(\phi+\varphi)] - \mu R$. It can be seen that the sign of f_d is determined by the sign of R'. R' is negative if the summation of items in the square brackets is negative. For a positive coefficient of R_w, increasing R_w will help to obtain a positive R'. As shown in Eq. (9), it can be achieved by increasing the mass ratio (m/M), eccentricity, or magnification factor. However, it must be pointed out that the increase of mass ratio can only be realized by reducing the total mass (or exactly, the stator mass) rather than increasing the rotor mass. The reason is that the increase of rotor mass means the decrease of the eccentricity if the imbalance remains unchanged.

The automatic balancing system used in a commercial CD-ROM is considered here as an example. The system parameters given in Table 1 are used in our numerical simulations. It should be pointed out that in the actual balancing system nine 90 mg balls are used, but the ball mass used here is 400 mg since only two balls are used in the time response analysis to be presented later. Also, for a CD-ROM, its initial imbalance is usually about 5 g mm; however, in the analysis here and imbalance of 1 g mm (as indicated in parentheses in Table 1) is assumed because our concern here is the steady state in which most of the initial imbalance has already been compensated by the balancing balls. Based on these parameters, R' value with respect to ball's angular position is calculated while the friction coefficient, rotating speed and mass ratio are varied. As indicated in Eq. (9), the eccentricity will have the same influence on R' as that of mass ratio; thus, it is not examined here.

Fig. 5 shows the influence of friction on R'. The rotating speed is fixed at 6000 rpm. For zero friction, R' over the whole racetrack are positive except at the two equilibriums positions where R' is zero. With the increase of friction, the curve translates downwards and makes the positive range smaller. This means that balls' probable settling area around the desired positions becomes wider and the automatic balancing effect is compromised. The effects of rotational speed are indicated in Fig. 6, in which the friction coefficient is fixed at 0.0002 for the purpose of simulation. At 2000 rpm, which is slightly higher than the critical speed, R' may become larger. However, the influence of speed on the range of positive R' is quite small. Especially for high speeds, their curves almost overlap because the speed only affects the magnification factor in the expression of whirling radius. In Fig. 7, the influence of mass ratio is presented. Note that the mass ratio is

Table 1
Used system parameter values

System parameters	Applied values
Total mass (M)	0.11 kg
Mass of rotating parts (m)	0.05 kg
Mass of balancing ball (m_b)	0.0004 kg
Radius (R)	0.013 m
Stiffness (k)	2711 N/m
Natural frequency (ω_n)	$\omega_n = \sqrt{K/M}$
Damping factor (ζ)	0.02
Imbalance	5 g mm (1 g mm)

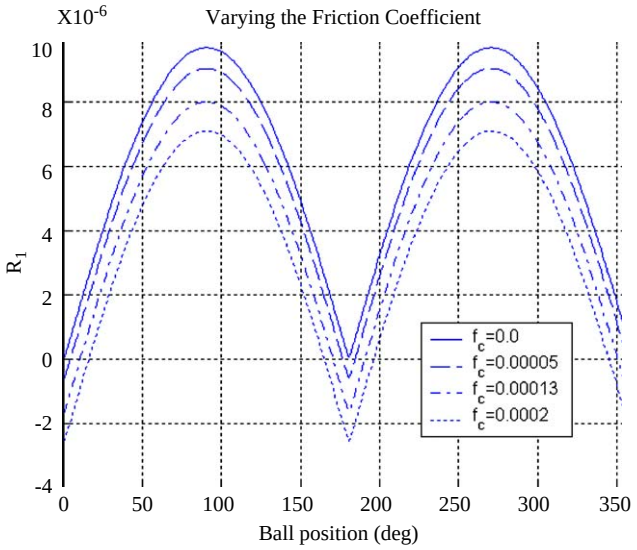

Fig. 5. Friction influence on R', $\Omega = 6000$ rpm.

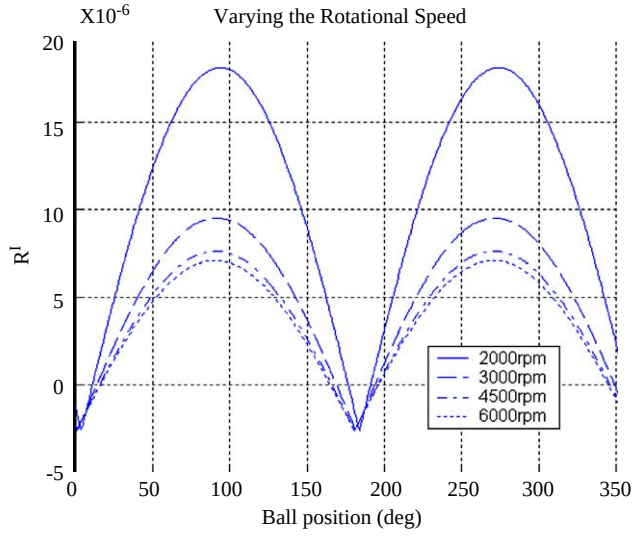

Fig. 6. Influence of rotating speed on R', $\mu = 0.0002$.

varied by changing the total mass while the masses of rotating parts remain unchanged. It is seen that increasing the mass ratio can widen the range of positive R' significantly, and consequently improve the automatic balancing effect. However, the limitation is that the maximum mass ratio is 1.

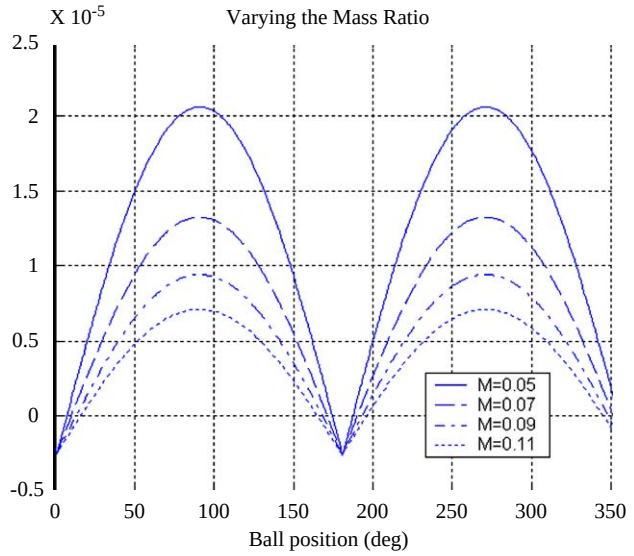

Fig. 7. Influence of mass ratio on R', $\Omega = 6000\,\text{rpm}$, $\mu = 0.0002$.

4. Time response

To further explore the influence of friction on the dynamic behavior of the system, the time responses are obtained by solving the equations of motion with a commercial software package, Matlab. The equations of motion are first established with respect to a fixed reference frame, and then transformed into the synchronous rotating frame, which are finally written in the form of state space.

4.1. Equations of motion

In time response analysis, the ball's movement in the racetrack must be included. Balls' rotation consists of two parts: one is the system's rotation around the whirling center O at a constant velocity of ω, and the other is the movement of the ball itself in the racetrack around the geometric center C with a relative speed of $\dot{\phi}_i$. Since the axes of these two rotations are parallel, balls' resultant rotational velocity is the sum of these two velocities, and its instantaneous resultant rotating center P keeps moving on the line CO. If two rotations are in the same direction, P will locate between C and O, as shown in Fig. 8(a). While two rotations are opposite, P will lie outside CO, either on the side O ($|\dot{\phi}| < \omega$) or on the side of C ($|\dot{\phi}| > \omega$). Let P_{Ci} denote the distance from C to P; we can then define the instantaneous position of P as

$$P_{Ci} = \frac{R_w \omega}{\omega + \dot{\phi}_i}. \tag{18}$$

The instantaneous rotating radius of the ball R_{Pi} and angle α_i can be expressed as

$$R_{Pi} = \sqrt{R^2 + P_{Ci}^2 - 2RP_{Ci}\cos\beta_i}, \tag{19}$$

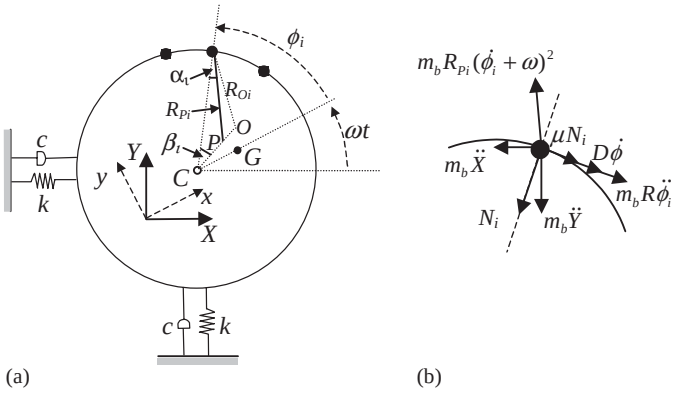

Fig. 8. Precise model for time response.

$$\cos\,\alpha_i = \frac{R - P_{Ci}\cos\,\beta_i}{R_{Pi}}, \tag{20}$$

$$\sin\,\alpha_i = \frac{P_{Ci}\sin\,\beta_i}{R_{Pi}}. \tag{21}$$

Considering the rotor and the balancing balls together, the equations of motion of the whole system with respect to the fixed frame can be obtained by modifying Eqs. (1) and (2)

$$M\ddot{X} + c\dot{X} + kX - m\varepsilon\omega^2\cos\,\omega t - m_b\sum_{i=1}^{n} R_{Pi}(\dot{\phi}_i + \omega)^2\cos(\phi_i + \omega t + \alpha_i) - m_b R\sum_{i=1}^{n}\ddot{\phi}_i\sin(\phi_i + \omega t) = 0, \tag{22}$$

$$M\ddot{Y} + c\dot{Y} + kY - m\varepsilon\omega^2\sin\,\omega t - m_b\sum_{i=1}^{n} R_{Pi}(\dot{\phi}_i + \omega)^2\sin(\phi_i + \omega t + \alpha_i) + m_b R\sum_{i=1}^{n}\ddot{\phi}_i\cos(\phi_i + \omega t) = 0. \tag{23}$$

Here, M is the total mass of the system. All the balls are assumed to have the same mass and located in a circular ring with a radius of R.

The forces, including inertia forces, acting on the ith balancing ball are indicated in Fig. 8(b). N_i is the normal force in the radial direction, and can be expressed as

$$N_i = m_b[R_{Pi}(\dot{\phi}_i + \omega)^2\cos\,\alpha_i - \ddot{Y}\sin(\phi_i + \omega t) - \ddot{X}\cos(\phi_i + \omega t)]. \tag{24}$$

Therefore, with the consideration of the frictional force the equations of motion for the balancing balls in the tangential direction can be written as

$$m_b[R\ddot{\phi}_i - R_{Pi}(\dot{\phi}_i + \omega)^2\sin\,\alpha_i + \ddot{Y}\cos(\phi_i + \omega t) - \ddot{X}\sin(\phi_i + \omega t)] + D\dot{\phi}_i + \mu m_b[R_{Pi}(\dot{\phi}_i + \omega)^2\cos\,\alpha_i - \ddot{Y}\sin(\phi_i + \omega t) - \ddot{X}\cos(\phi_i + \omega t)] = 0, \quad i = 1, 2, \ldots, n \tag{25}$$

where D is the viscous drag coefficient and can be similarly defined as in Ref. [3]

$$D = vm_b R\omega_n, \tag{26}$$

in which v is the non-dimensional coefficient.

To obtain the equations in a time-independent form, a synchronous rotating frame, in which the x-axis is parallel to CG, is introduced, as shown in Fig. 8(a). Transforming the equations of motion (22), (23) and (25) from fixed frame into rotating frame [6], we have

$$\begin{aligned}&(M + nm_b)(\ddot{x} - 2\omega\dot{y} - \omega^2 x) - m\varepsilon\omega^2 + c\dot{x} - c\omega y + kx\\ &\quad - m_b \sum_{i=1}^{n} R_{Pi}(\dot{\phi}_i + \omega)^2 \cos(\phi_i + \alpha_i) - m_b R \sum_{i=1}^{n} \ddot{\phi}_i \sin \phi_i = 0,\end{aligned} \tag{27}$$

$$\begin{aligned}&(M + nm_b)(\ddot{y} + 2\omega\dot{x} - \omega^2 y) + c\dot{y} + c\omega x + ky\\ &\quad - m_b \sum_{i=1}^{n} R_{Pi}(\dot{\phi}_i + \omega)^2 \sin(\phi_i + \alpha_i) + m_b R \sum_{i=1}^{n} \ddot{\phi}_i \cos \phi_i = 0,\end{aligned} \tag{28}$$

$$\begin{aligned}&m_b[R\ddot{\phi}_i - R_{Pi}(\dot{\phi}_i + \omega)^2 \sin \alpha_i + (\ddot{y} + 2\omega\dot{x} - \omega^2 y)\cos \phi_i - (\ddot{x} - 2\omega\dot{y} - \omega^2 x)\sin \phi_i] + D\dot{\phi}_i\\ &\quad + \mu m_b[R_{Pi}(\dot{\phi}_i + \omega)^2 \cos \alpha_i - (\ddot{y} + 2\omega\dot{x} - \omega^2 y)\sin \phi_i - (\ddot{x} - 2\omega\dot{y} - \omega^2 x)\cos \phi_i] = 0,\\ &\qquad i = 1, 2, \ldots, n.\end{aligned} \tag{29}$$

4.2. State space equations

In order to solve the differential equations of motion by Matlab, the equations of motion (27)–(29) are written in the standard form of

$$P(u)\dot{u} = Q(u), \tag{30}$$

where

$$u = [x, y, \phi_1, \phi_2, \ldots, \phi_n, \dot{x}, \dot{y}, \dot{\phi}_1, \dot{\phi}_2, \ldots, \dot{\phi}_n]^{\mathrm{T}} \tag{31}$$

and

$$P(u) = \begin{bmatrix} I & 0 \\ M & N \end{bmatrix}, \tag{32}$$

in which I is the $(n+2) \times (n+2)$ identity matrix and

$$M = \begin{bmatrix} c & -2\omega(M + nm_b) & 0 & 0 & \cdots & 0 \\ 2\omega(M + nm_b) & c & 0 & 0 & \cdots & 0 \\ 2m_b\omega(C_1 - \mu S_1) & 2m_b\omega(S_1 + \mu C_1) & D & 0 & \cdots & 0 \\ 2m_b\omega(C_2 - \mu S_2) & 2m_b\omega(S_2 + \mu C_2) & 0 & D & \cdots & 0 \\ \vdots & \vdots & \vdots & \vdots & \ddots & \vdots \\ 2m_b\omega(C_n - \mu S_n) & 2m_b\omega(S_n + \mu C_n) & 0 & 0 & \cdots & D \end{bmatrix}, \tag{33}$$

$$N = \begin{bmatrix} M + nm_b & 0 & -m_b RS_1 & -m_b RS_2 & \cdots & -m_b RS_n \\ 0 & M + nm_b & m_b RC_1 & m_b RC_2 & \cdots & m_b RC_n \\ m_b(-\mu C_1 - S_1) & m_b(C_1 - \mu S_1) & m_b R & 0 & \cdots & 0 \\ m_b(-\mu C_2 - S_2) & m_b(C_2 - \mu S_2) & 0 & m_b R & \cdots & 0 \\ \vdots & \vdots & \vdots & \vdots & \ddots & \vdots \\ m_b(-\mu C_n - S_n) & m_b(C_n - \mu S_n) & 0 & 0 & \cdots & m_b R \end{bmatrix} \tag{34}$$

and

$$Q(u) = \begin{bmatrix} \dot{x} \\ \dot{y} \\ \dot{\phi}_1 \\ \dot{\phi}_2 \\ \vdots \\ \dot{\phi}_n \\ [\omega^2(M + nm_b) - k]x + c\omega y + m\varepsilon\omega^2 + m_b \sum_{i=1}^{n} R_{Pi}(\dot{\phi}_i + \omega)^2 C_{\phi\alpha_i} \\ [\omega^2(M + nm_b) - k]y - c\omega x + m_b \sum_{i=1}^{n} R_{Pi}(\dot{\phi}_i + \omega)^2 S_{\phi\alpha_i} \\ m_b\omega^2(yC_1 - xS_1 - \mu xC_1 - \mu yS_1) + m_b R_{Pi}(\dot{\phi}_1 + \omega)^2(S_{\alpha 1} - \mu C_{\alpha 1}) \\ m_b\omega^2(yC_2 - xS_2 - \mu xC_2 - \mu yS_2) + m_b R_{Pi}(\dot{\phi}_2 + \omega)^2(S_{\alpha 2} - \mu C_{\alpha 2}) \\ \vdots \\ m_b\omega^2(yC_n - xS_n - \mu xC_n - \mu yS_n) + m_b R_{Pi}(\dot{\phi}_n + \omega)^2(S_{\alpha n} - \mu C_{\alpha n}) \end{bmatrix}. \tag{35}$$

In Eqs. (33)–(35), we have

$$\begin{aligned} &C_i = \cos\,\phi_i, \quad S_i = \sin\,\phi_i, \quad C_{\alpha i} = \cos\,\alpha_i, \quad S_{\alpha i} = \sin\,\alpha_i, \\ &C_{\phi\alpha_i} = \cos(\phi_i + \alpha_i), \quad S_{\phi\alpha_i} = \sin(\phi_i + \alpha_i). \end{aligned} \tag{36}$$

Then the state equations are expressed as in the form of

$$\dot{u} = P(u)^{-1} Q(u). \tag{37}$$

4.3. Numerical results of time analyses

Based on the analysis in Section 4.2, a Matlab program is written to solve the differential equations. ODE23 is chosen as the solver for the sake of simplicity. The basic parameters listed in Table 1 in Section 3 are also applied in the time response analyses. Without losing generality, the case with two balancing balls is considered. In the simulation, the system's initial displacements

and velocities in both x and y directions are given by zero. With two balls, an initial velocity of 10 rad/s is applied to both $\dot{\phi}_1$ and $\dot{\phi}_2$, and their initial positions are varying in our analyses. It is worth pointing out that the gravity center shift caused by the ball's movement is also considered in our analyses.

4.3.1. With viscous drag force only

First, the time response analysis is carried out with the assumption of zero friction ($\mu = 0$). For the non-dimensional viscous drag coefficient, $v = 0.01$ is given. Fig. 9 shows the results with the initial ball position of $[-\pi/4, \pi]$, and a rotational speed of 600 rpm ($\omega/\omega_n = 0.4$). The steady whirling radius is 26.7256 μm. Two balls are located at the same position of -3.3664° (-0.0588 rad). This coincides with the conclusion drawn in Section 3 which states that the stable equilibrium position will approach the location of imbalance if $\omega/\omega_n \ll 1$. In Fig. 10, the rotational speed is increased to 6000 rpm. The system is perfectly balanced and the final whirling radius is 5.4671e-4 μm. Two balls stay at $[\pm 118.7356^\circ]$ ($[\pm 2.0723$ rad]), which are considered to be the desired positions. The simulation with only viscous drag force is also undertaken with many other different initial positions. For all of them, the system can be perfectly balanced with two balls settled at $[\pm 118.7356^\circ]$ and the steady whirling radius of less than 1 nm.

4.3.2. With both viscous drag and frictional forces

Even though an ABB has fluid filled in the racetrack, the frictional force cannot be neglected because the balls are pressed against the sidewall of the racetrack by the centrifugal forces. Especially with the system approaching the steady state, the viscous drag force becomes smaller while the friction remains unchanged. Fig. 11 indicates the time response when $v = 0.01$, $\mu = 0.00005$ and $\Omega = 600$ rpm, two balls stay at $[0.6617^\circ, -2.0283^\circ]$ and the final whirling radius is 26.73 μm. Compared with Fig. 9, it is seen that the time to reach steady state is shorter in this case because of friction. If the friction is further increased to $\mu = 0.0002$ at $\Omega = 600$ rpm, the results show a similar trend as in the case of $\mu = 0.00005$, but only take 4 s to reach steady state; the balls' final locations are $[-6.7211^\circ, -13.0621^\circ]$ and steady whirling radius is 26.6203 μm.

Increasing the rational speed to 6000 rpm, the results for $v = 0.01$ and $\mu = 0.00005$ are presented in Fig. 12. Two balls settle at $[-118.2970^\circ, 118.8605^\circ]$, and the steady whirling radius is

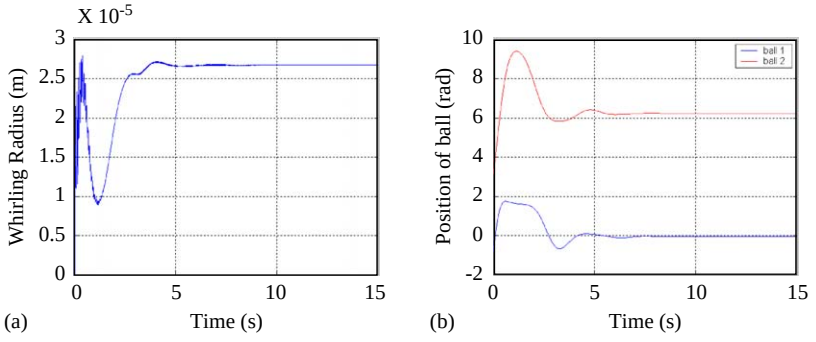

Fig. 9. Time histories of (a) whirling radius and (b) balls' displacements, when $v = 0.01$, $\mu = 0$, $\Omega = 600$ rpm, ini. pos. $[-\pi/4, \pi]$.

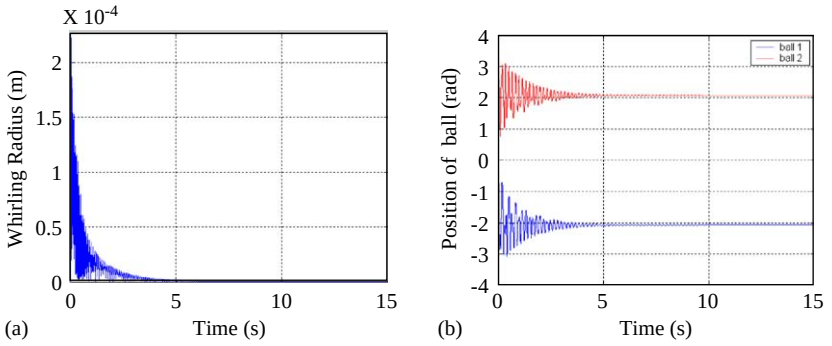

Fig. 10. Time histories of (a) whirling radius and (b) balls' displacements, when $v = 0.01$, $\mu = 0$, $\Omega = 6000$ rpm, ini. pos $[-\pi/4, \pi]$.

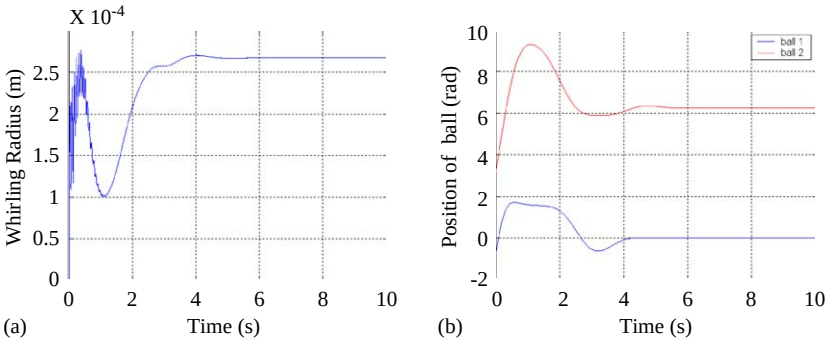

Fig. 11. Time histories of (a) whirling radius and (b) balls' displacements, when $v = 0.01$, $\mu = 0.00005$, $\Omega = 600$ rpm, ini. pos $[-\pi/4, \pi]$.

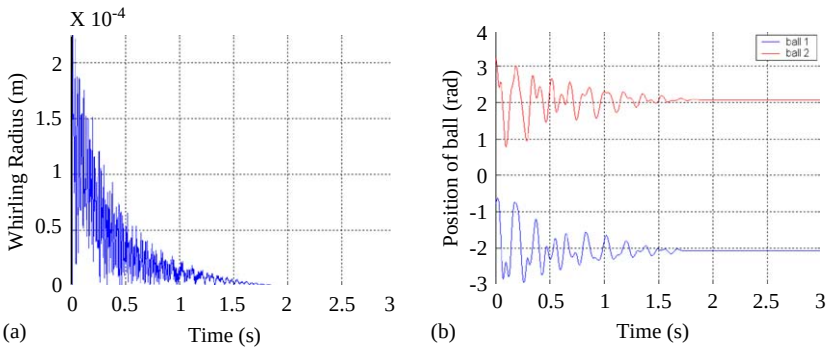

Fig. 12. Time histories of (a) whirling radius and (b) balls' displacements, when $v = 0.01$, $\mu = 0.00005$, $\Omega = 6000$ rpm, ini. pos $[-\pi/4, \pi]$.

0.343 μm. Compared to the case indicated in Fig. 10, the balancing effect is compromised and the balancing time is more than three times shorter, reducing from 6 to 1.8 s. Increasing the friction to $\mu = 0.0002$, the time response is then shown in Fig. 13. Balls' final positions are at

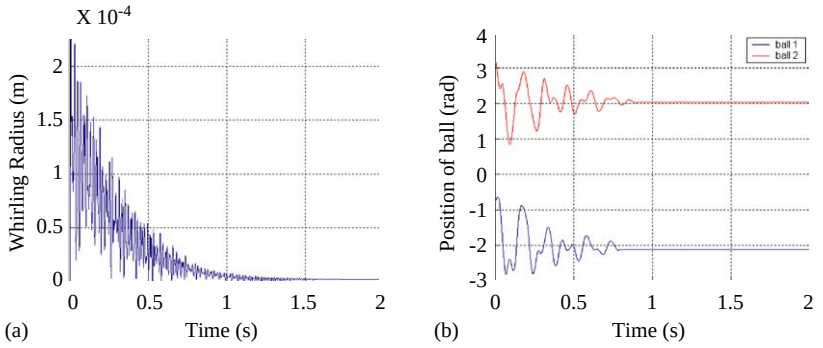

Fig. 13. Time histories of (a) whirling radius and (b) balls' displacements, when $v = 0.01$, $\mu = 0.0002$, $\Omega = 6000$ rpm, ini. pos $[-\pi/4, \pi]$.

$[-121.5027°, 116.9006°]$ and the steady whirling radius is 2.0886 μm. It is seen that the balancing effect is further compromised and it only takes 0.8 s for the balls to settle.

Note that with some initial ball positions, the system can still be balanced quite well even for a high friction coefficient, as the balls' final positions are actually random over a range in the vicinity of the desired positions. In order to avoid the misconception caused by the contingency of an individual case, the time responses with different frictions are obtained for 15 cases in which two balls have different initial positions. By means of the statistical results of these 15 cases, the influence of friction on the balancing effect will become more straightforward. In Table 2, the balls' final locations and system's steady whirling radii for 15 different cases are listed. As it is known, for the final positions of both balls, normally one gets a positive value and the other a negative value when the imbalance is taken as the reference. Therefore, in the calculation of average and standard deviation of position values of all 15 cases, two balls are taken into consideration together and absolute values are used in order to ensure that the positive and negative values do not cancel out each other. As indicated in Table 2, there is no significant difference when friction increases from $\mu = 0.00003$ to 0.00005, and then, with the friction further increasing to $\mu = 0.00013$ and 0.00002, the balancing effect is compromised further.

To diagrammatically show balls' possible distribution region in steady state under different frictions, the final locations of two balls for these 15 cases are drawn in the same figure. As shown in Fig. 14, the distribution ranges of two balls for $\mu = 0.00003$ is slightly larger than that for $\mu = 0.00005$. From $\mu = 0.00005$ to 0.0002, with the increase of friction the possible dwelling ranges of two balls increase as well.

4.3.3. With friction only

For an ABB without fluid filled in the racetrack, such as the one found in the commercial CD-ROM, the viscous drag force of air can be neglected and so we have $v = 0$. In this circumstance, the friction plays a key role for balls in approaching their desired positions. Fig. 15 indicates the time response when $\mu = 0.00005$, $\Omega = 600$ rpm and balls' initial positions are $[-\pi/4, \pi]$. It takes about 1 min for the balls to settle at $[-0.8720°, -2.4132°]$, and the system's steady whirling radius is 26.732 μm. If friction $\mu = 0.0002$ is applied, then for $\Omega = 600$ rpm, the two balls take less than 20 s to settle at $[-39.3552°, -23.7555°]$ with a steady whirling radius of

Table 2
Simulation results for 15 cases with different initial ball positions and friction coefficients ($v = 0.01$, $\Omega = 6000$ rpm)

Ini. pos of 15 different cases	$\mu = 0.00003$			$\mu = 0.00005$			$\mu = 0.00013$			$\mu = 0.0002$		
	Final ball pos.(rad)		Final whirl (μm)	Final ball pos.(rad)		Final whirl (μm)	Final ball pos.(rad)		Final whirl (μm)	Final ball pos.(rad)		Final whirl (μm)
	Ball 1	Ball 2		Ball 1	Ball 2		Ball 1	Ball 2		Ball 1	Ball 2	
$-\pi/4, \pi$	−2.078	2.065	0.333	−2.065	2.075	0.343	−2.096	2.064	1.014	−2.121	2.040	2.089
$\pi/4, \pi$	2.077	−2.066	0.268	2.063	−2.083	0.472	2.032	−2.157	3.640	1.144	−2.541	32.568
$3\pi/5, -\pi/3$	2.090	−2.061	0.776	2.074	−2.060	0.601	2.072	−2.073	0.027	−2.051	2.090	0.965
$-\pi/3, -\pi/5$	−2.073	2.064	0.391	−2.041	2.127	2.353	−2.050	2.094	1.067	−2.052	2.093	1.006
$\pi/6, 4\pi/5$	2.076	−2.063	0.404	2.121	−2.042	2.082	−2.109	2.008	2.703	2.073	−2.071	0.056
$5\pi/4, 3\pi/4$	−2.079	2.065	0.353	−2.073	2.072	0.040	−2.072	2.072	0.017	−2.074	2.070	0.105
$0, \pi$	2.073	−2.076	0.189	2.075	−2.064	0.352	2.006	−2.225	6.664	2.352	−1.878	12.419
$-\pi/6, 4\pi/5$	2.072	−2.071	0.059	−2.063	2.087	0.623	2.260	−1.731	13.648	−1.784	2.227	11.649
$-4\pi/5, -\pi/7$	−2.13	2.043	2.467	2.061	−2.081	0.478	−2.261	1.964	8.203	−2.258	1.705	14.649
$3\pi/8, -\pi/2$	2.074	−2.072	0.094	2.075	−2.075	0.225	−2.695	1.657	28.446	−2.114	2.018	2.381
$\pi/2, -5\pi/12$	−2.065	2.084	0.496	2.079	−2.062	0.417	2.073	−2.062	0.471	−2.044	2.154	3.567
$11\pi/10, 2\pi/5$	−2.07	2.072	0.14	−1.850	2.194	9.095	−2.111	1.993	3.337	−2.122	2.000	3.077
$\pi/6, \pi/8$	2.08	−2.067	0.32	2.055	−2.080	0.753	−2.091	2.060	0.799	−1.831	2.474	17.939
$-5\pi/8, 2\pi/3$	−2.078	2.066	0.293	−2.080	2.058	0.624	−2.019	2.095	2.257	−2.132	1.982	3.817
$-\pi/5, 8\pi/11$	−1.93	2.342	11.871	−2.060	2.083	0.568	2.051	−2.074	1.048	2.152	−2.035	3.457
Average	2.0774		1.2303	2.0691		1.2684	2.0775		4.8894	2.0561		7.3162
Std dev	0.0580		3.0004	0.0502		2.2585	0.1675		7.5093	0.2442		9.0428

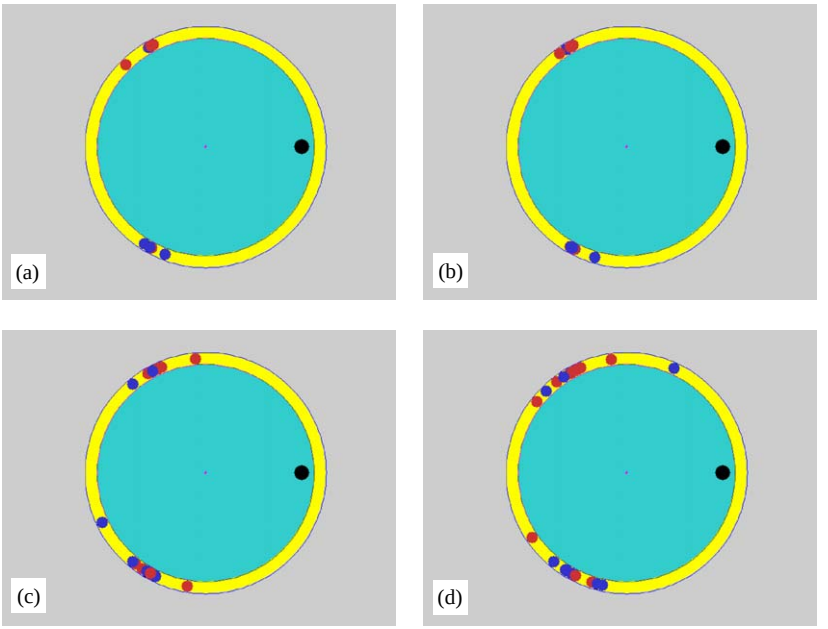

Fig. 14. Balls' distribution for 15 cases ($v = 0.01$, $\Omega = 6000$ rpm). (a) $\mu = 0.00003$, (b) $\mu = 0.00005$, (c) $\mu = 0.00013$, (d) $\mu = 0.0002$.

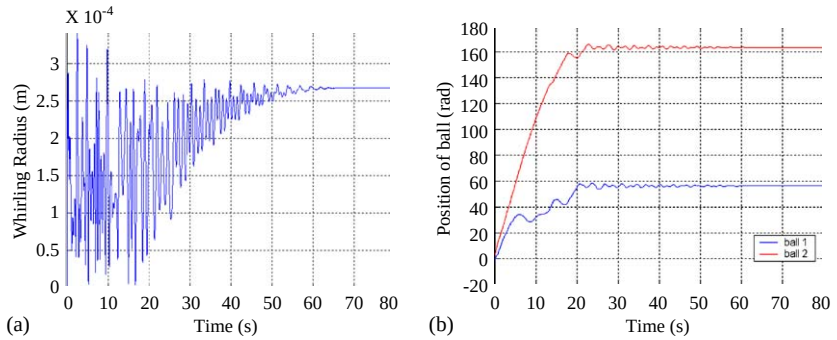

Fig. 15. Time histories of (a) whirling radius and (b) balls' displacements, when $v = 0$, $\mu = 0.00005$, $\Omega = 600$ rpm, ini. pos $[-\pi/4, \pi]$.

25.686 μm. Increasing the rotational speed to 6000 rpm, the results for $\mu = 0.00005$ are given in Fig. 16. The balls' final positions are at $[-118.2810^\circ, 118.6986^\circ]$ and the steady whirling radius is 0.4188 μm. If the friction coefficient is then increased to $\mu = 0.0002$, as shown in Fig. 17, the balls take less time to settle down and the final locations are $[-120.8620^\circ, 116.0317^\circ]$ with a steady whirling radius of 2.0648 μm.

Without considering the viscous drag force, time response analyses are also carried out for the 15 cases in Section 4.3.1. The results are presented in Table 3. The balancing effects for different frictions are indicated by the corresponding average and standard deviation values and also, the dwelling ranges of two balls as shown in Fig. 18. It is interesting that the balancing effect for

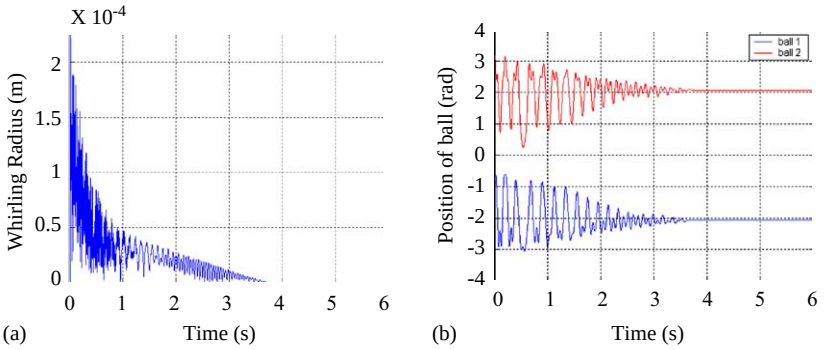

Fig. 16. Time histories of (a) whirling radius and (b) balls' displacements, when $v = 0$, $\mu = 0.00005$, $\Omega = 6000$ rpm, ini. pos $[-\pi/4, \pi]$.

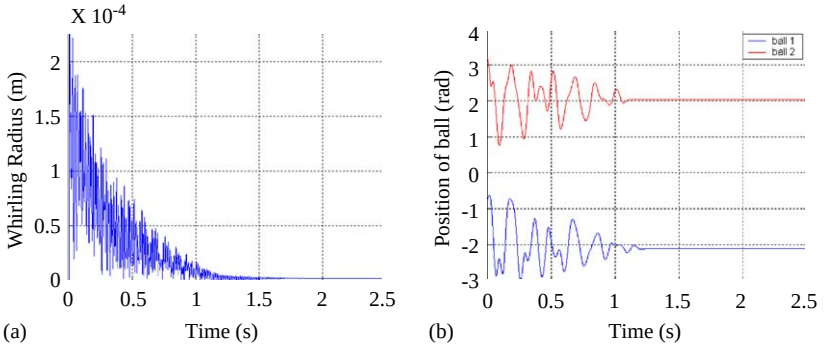

Fig. 17. Time histories of (a) whirling radius and (b) balls' displacements when $v = 0$, $\mu = 0.0002$, $\Omega = 6000$ rpm, ini. pos $[-\pi/4, \pi]$.

$\mu = 0.00005$ is better than that for $\mu = 0.00003$. This can be explained by the fact that with too low a friction the ball cannot stop in time when it passes through the desired positions; as an example, the system would not reach a steady state in the extreme case of $\mu = 0$ because the ball keeps moving. For the cases $\mu = 0.00013$ and 0.0002, the balls' dwelling ranges become wider and balancing effects degrade with the increase of friction. These results suggest that there is an optimal point or range for the friction in the automatic ball balancing system.

In particular, when $\mu = 0.0002$ there is a case with initial ball positions $[\pi/6, \pi/8]$ whereby one ball finally stays almost opposite the initial imbalance and the other very near the imbalance. As explained in Section 3, these positions are very close to the two equilibriums and hence the driving forces acting on them are very small. Although the one near the imbalance is an unstable one, the ball can still stay there due to friction and no disturbance.

Comparing the simulation results between the cases with and without viscous drag force, for $\mu = 0.00005$ and 0.00013, it is seen that the cases without viscous drag force have better balancing effects, while for $\mu = 0.00003$ and 0.0002, it seems that the cases with viscous drag force can yield better results.

Table 3
Simulation results for cases with different initial ball positions and friction coefficients ($v = 0$, $\Omega = 6000$ rpm)

Ini. pos of 15 different cases	$\mu = 0.00003$			$\mu = 0.00005$			$\mu = 0.00013$			$\mu = 0.0002$		
	Final ball pos.(rad)		Final whirl (μm)	Final ball pos.(rad)		Final whirl (μm)	Final ball pos.(rad)		Final whirl (μm)	Final ball pos.(rad)		Final whirl (μm)
	B1	B2		B1	B2		B1	B2		B1	B2	
$-\pi/4, \pi$	2.064	−2.075	0.361	−2.064	2.072	0.419	−1.676	2.284	15.706	−2.109	2.025	2.065
$\pi/4, \pi$	2.064	−2.078	0.37	2.059	−2.085	0.632	2.138	−1.927	6.073	2.095	−2.064	0.972
$3\pi/5, -\pi/3$	2.071	−2.068	0.269	−2.104	2.05	1.388	−2.01	2.122	2.757	−1.994	2.117	3.286
$-\pi/3, -\pi/5$	2.192	−2.079	5.186	−2.068	2.08	0.309	−2.144	1.946	5.256	−2.156	1.921	6.262
$\pi/6, 4\pi/5$	2.058	−2.079	0.621	2.063	−2.068	0.65	−2.129	2.058	2.535	−1.531	3.005	43.495
$5\pi/4, 3\pi/4$	−2.079	2.060	0.515	−2.056	2.082	0.698	−2.081	2.068	0.354	−2.074	2.072	0.0599
$0, \pi$	−2.065	2.086	0.566	−2.078	2.067	0.256	2.063	−2.077	0.408	1.891	−2.42	15.462
$-\pi/6, 4\pi/5$	−1.795	2.222	11.225	−2.073	2.073	0.056	−2.170	1.890	7.49	−1.963	2.119	4.611
$-4\pi/5, -\pi/7$	−2.068	2.072	0.245	2.075	−2.068	0.203	2.089	−2.032	1.716	2.194	−1.987	5.309
$3\pi/8, -\pi/2$	−1.986	2.235	7.068	−2.065	2.071	0.439	2.072	−2.07	0.126	2.087	−2.067	0.639
$\pi/2, -5\pi/12$	2.083	−2.055	0.737	−2.054	2.089	0.84	2.101	−2.034	1.657	1.049	−2.606	34.995
$11\pi/10, 2\pi/5$	−2.072	2.078	0.302	−2.061	2.096	1.238	−2.177	1.89	7.507	−2.218	1.816	10.447
$\pi/6, \pi/8$	−2.08	2.07	0.352	2.063	−2.083	0.503	2.227	−1.778	11.877	3.035	−0.194	47.649
$-5\pi/8, 2\pi/3$	−2.082	2.051	0.894	−2.063	2.084	0.507	−2.007	2.118	2.805	−2.129	1.971	4.205
$-\pi/5, 8\pi/11$	−2.055	2.107	1.467	−2.063	2.078	0.38	−2.072	2.075	0.123	−2.073	2.07	0.0805
Average	2.0743		2.0119	2.0718		0.5679	2.0508		4.426	2.0351		11.9692
Std dev	0.0721		2.1328	0.0124		0.3650	0.1249		4.6196	0.4997		16.2765

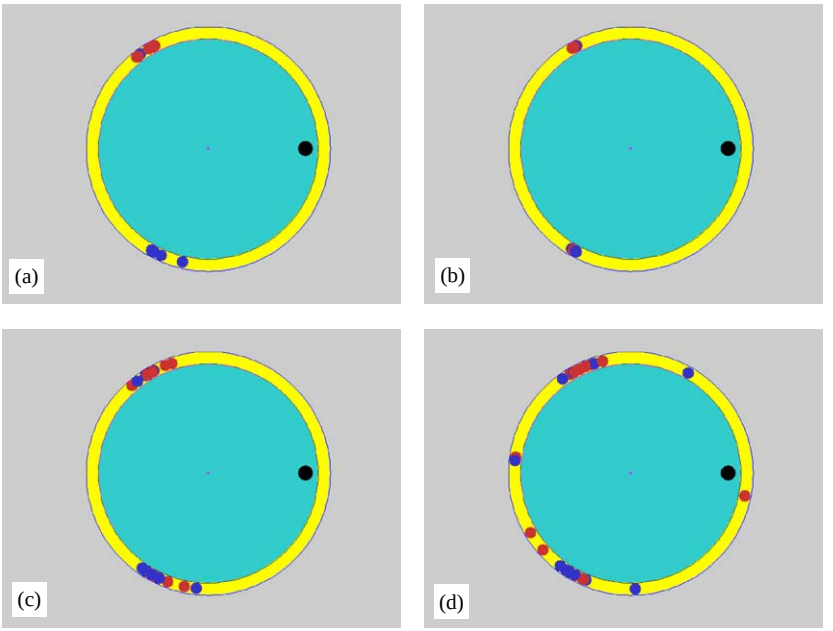

Fig. 18. Balls' distribution for 15 cases, ($v = 0, \Omega = 6000$ rpm). (a) $\mu = 0.00003$, (b) $\mu = 0.00005$, (c) $\mu = 0.00013$, (d) $\mu = 0.0002$.

In the simulations that consider only the friction, the system cannot reach a steady state for some initial ball positions. However, the results show that they always fall into the oscillatory steady state. In this state, both balls keep moving in the racetrack in a direction opposite to the system rotation. (In some cases, only one ball keeps moving while the other oscillates with a very small amplitude around an equilibrium position. It must be mentioned that this kind of oscillatory steady state can only occur in the simulation but not in practice, because the impact between two balls is not considered in simulation and therefore, one ball can pass through the other without affecting each other.) An important feature is that their velocities will asymptotically approach certain values in an oscillatory manner, with the same period but out of phase to each other. As an example, Fig. 19 shows the simulation results for a case with $\mu = 0.00005$, rotating speed 6000 rpm, and the initial ball positions of $[-\pi/4, 3\pi/8]$. It is seen that there is a drastic change in behavior, as illustrated by a large peak in Fig. 19(a), before the system enters the oscillatory steady state. After that, the first ball comes to a steady oscillation with a very small amplitude around its equilibrium position, while the other keeps moving in the racetrack opposite to the system rotation. As indicated in Figs. 19(d) and (e), which show the velocity of two balls in steady state in detail, their phases are opposite to each other. For the second ball, its velocity will finally approach a certain value. Although we cannot tell what this value will be, it is expected not to exceed the system's rotational speed. This conjecture can be explained by means of Fig. 8, once $|\dot{\phi}| > \omega$, the ball's instantaneous rotating center P will suddenly move from the infinite on the right of O to somewhere near the left of C and the ball's resultant velocity also reverses. Consequently, the driving force now becomes the resistance to the ball.

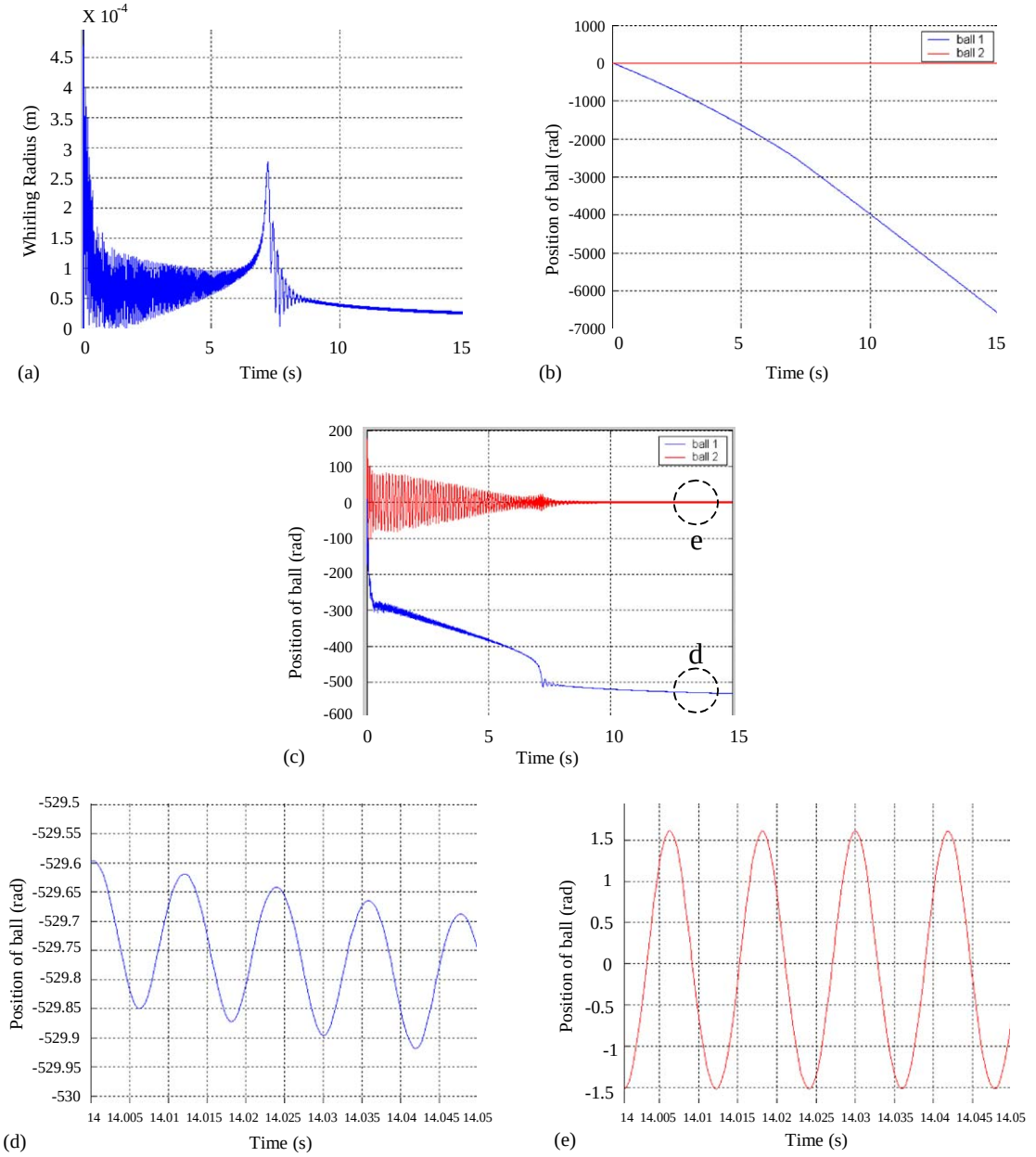

Fig. 19. Oscillatory steady state, $v = 0.01$, $\mu = 0.00005$, $\Omega = 6000$ rpm, ini. pos $[-\pi/4, 3\pi/8]$. (a) Whirling radius, (b) Ball's displacements, (c) Ball's velocity, (d) velocity of ball 1, (e) velocity of ball 2.

Taking one ball into consideration, if its own velocity $\dot{\phi}$ is opposite to the system's rotation ω, with the increase of $|\dot{\phi}|$ its instantaneous radius of the resultant rotation and the angle α will also increase since the instantaneous resultant rotating center moves away from CO on the side of O, as indicated in Fig. 8 and Eqs. (18)–(21). This tends to generate a larger driving force. By chance,

if the movement of the other ball has the same period but just out of phase, it will cause the gravity center G and whirling line CO to change their positions with the same period. As a result, the increase in velocity of the first ball will be greater than the decrease over a circle, and hence will continue increasing the velocity. On the other hand, the resultant velocity of the ball will decrease with the increase of $\dot{\phi}$, resulting in a smaller centrifugal force and in turn, a smaller driving force. Finally, it will come to an end, and the oscillatory steady state is formed. From the simulations, it has been found that the oscillatory steady state occurs less frequently with the increase of friction.

To disrupt the oscillatory steady state, it is necessary to introduce a disturbance. This can be realized easily by running the motor near the critical speed for a while. For instance, in the previous case, set the motor speed set at 1530 rpm (51π rad/s) at the 10th second, and then go back to 6000 rpm in 3 s. As indicated in Fig. 20, the oscillatory steady state is disrupted by the severe disturbance at 1530 rpm, and the system then arrives at a steady state when the speed is restored to 6000 rpm. The final whirling radius is 1.1899 μm and the balls' final positions are [117.5680°, −120.2938°]. This method can also be applied in cases with high residual imbalance.

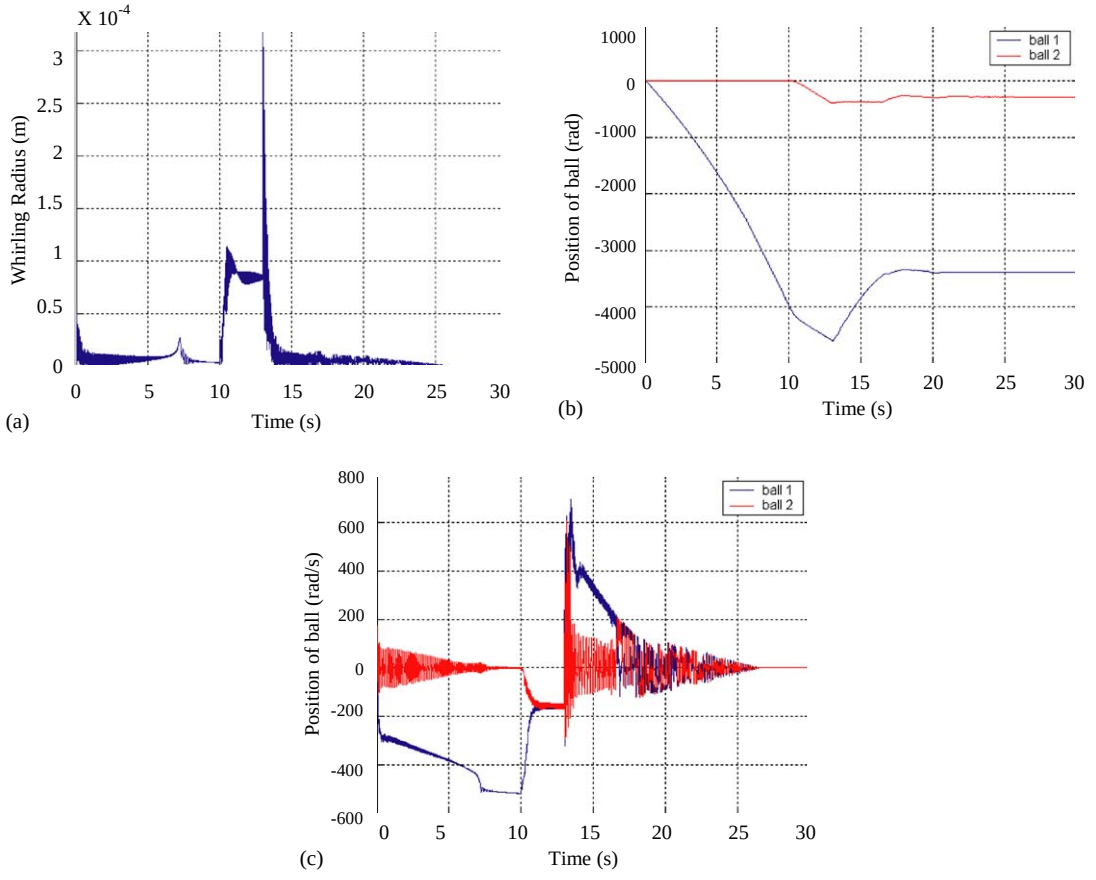

Fig. 20. Break of oscillatory steady state. (a) Whriling radius, (b) Ball's displacements, (c) Ball's velocity.

Table 4
Steady whirling radius (μm) with different ball masses ($\Omega = 6000$ rpm)

Ini. pos.	$v = 0$, $\mu = 0.0002$				$v = 0.01$, $\mu = 0.0002$			
	200 mg	300 mg	400 mg	500 mg	200 mg	300 mg	400 mg	500 mg
$-\pi/4$, π	1.567	3.312	2.065	13.991	0.423	2.635	2.089	1.189
$\pi/4$, π	0.843	1.081	0.972	3.358	0.015	0.324	32.568	3.948
$3\pi/5$, $-\pi/3$	0.654	0.976	3.286	2.024	1.815	0.093	0.965	1.893
$-\pi/3$, $-\pi/5$	0.432	1.002	6.262	8.010	1.857	9.506	1.006	7.001
$\pi/6$, $4\pi/5$	2.670	1.440	43.495	8.088	0.674	0.009	0.056	1.045
$5\pi/4$, $3\pi/4$	0.686	0.181	0.0599	0.969	1.157	0.236	0.105	0.024
0, π	5.702	2.087	15.462	2.639	0.257	0.078	12.419	0.807
$-\pi/6$, $4\pi/5$	0.319	0.196	4.611	1.750	0.064	5.581	11.649	0.305
$-4\pi/5$, $-\pi/7$	1.321	0.965	5.309	11.418	0.424	0.301	14.649	10.406
$3\pi/8$, $-\pi/2$	0.783	1.214	0.639	2.286	0.300	0.579	2.381	0.913
$\pi/2$,$-5\pi/12$	3.852	1.720	34.995	11.390	1.206	0.330	3.567	2.985
$11\pi/10$, $2\pi/5$	2.042	0.961	10.447	2.283	1.293	0.974	3.077	5.220
$\pi/6$, $\pi/8$	2.009	2.494	47.649	2.027	2.027	1.348	17.939	37.388
$-5\pi/8$, $2\pi/3$	0.415	0.177	4.205	3.155	1.116	0.031	3.817	0.029
$-\pi/5$, $8\pi/11$	1.407	0.836	0.0805	2.894	1.546	0.766	3.457	3.340
Average	1.6468	1.2429	11.9692	5.0854	0.9451	1.5193	7.3162	5.0997
Std dev	1.4848	0.8729	16.2765	4.2822	0.6831	2.6443	9.0428	9.3947

Utilizing the severe disturbance generated by the motor near the critical speed, the balls can be relocated at more desired positions to reduce the residual imbalance.

4.3.4. The influence of ball mass on the balancing effect

In an automatic ball balancing system, the ball mass is the most important design parameter. To further investigate the effects of ball mass, the time response analyses are performed for 15 cases with different initial positions, v and μ, as shown in Table 4. The final ball positions are not listed because with the use of different ball masses the balls' desired final positions are also different and no longer comparable. As indicated in this table, for a ball mass of 400 mg, which was used in our previous discussions, the balancing effects are worst. In general, we can see that using a relatively small ball mass tends to generate a better balancing effect.

Although our discussion here focuses on a two-ball case, we acknowledge that it is not too difficult a task to obtain the time response of multi-ball systems.

5. Experimental study

To verify the theoretical and numerical analyses, the experimental study is then carried out. As we know, the vibration amplitude caused by the imbalance in a system is proportional to the imbalance itself. Therefore, in our experiment the imbalance of the disk/motor pack was indirectly verified by measuring the vibration amplitude of the system with a laser doppler vibrometer (LDV).

5.1. Experimental setup

Fig. 21 shows the schematic diagram of the experimental setup. It is slightly different from the actual configuration in the commercial CD-ROM. As shown in Fig. 22, the disk/motor pack is mounted on a holder and supported by two thin aluminum shafts. Besides its simplicity, one main advantage of this setup is that it is an axisymmetric body so that it is very close to our theoretical model. A metal ring with a groove was mounted on the disk and secured firmly by a clamp. The clamp is made of Perspex and has two openings (see Fig. 23) on it to facilitate adding and removing balls without changing the system parameters such as assembly imbalance.

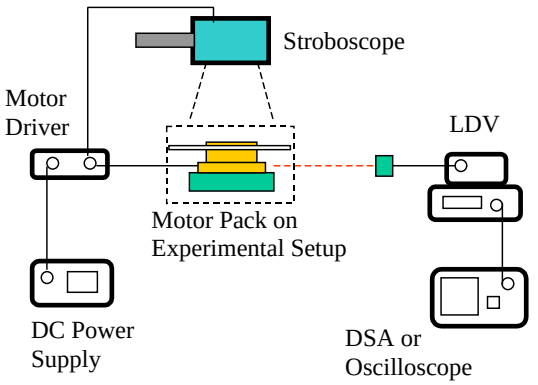

Fig. 21. The block diagram of the experimental configuration.

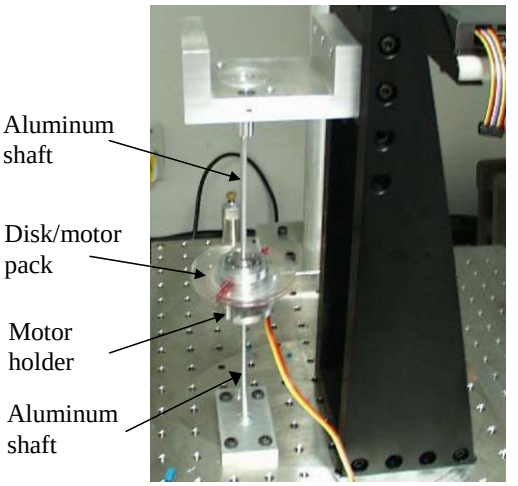

Fig. 22. Photograph of the experimental setup.

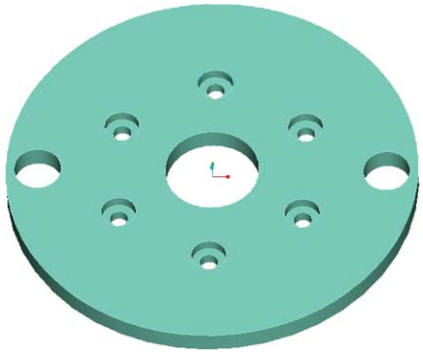

Fig. 23. The modified clamp with two holes.

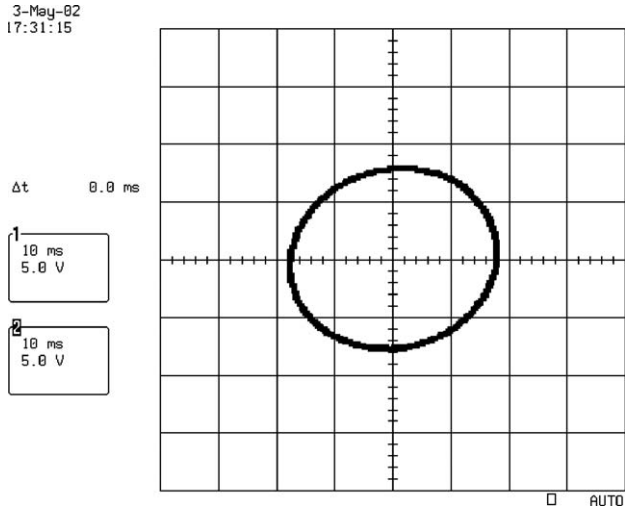

Fig. 24. Whirling circle of the setup.

5.2. *Verification of whirling motion*

The whirling motion of the system was verified by means of two LDVs. Two laser beams were projected onto two points at the same height but 90° apart. The signals obtained were then shown with an oscilloscope as in Fig. 24. It is quite smooth and circular.

5.3. *Experimental results*

Table 5 illustrates the experimental results of 20 consecutive measurements with varying frictional forces. In this experiment, we first balanced the system to make sure that the vibration level was very low, and then 0.076 g of plasticine was added on an arbitrary point at radius 30.8 mm of the disk to create an initial imbalance ($0.076\,\text{g} \times 30.8\,\text{mm} = 2.34\,\text{g mm}$). The initial

Table 5
Effects of friction on automatic balancing

Measurement number	Vibration amplitude in mV rms		
	W/o oil film	With thin oil film	With thick oil film
1	196.773	191.832	210.744
2	191.473	212.801	202.186
3	196.059	193.23	198.325
4	192.228	190.216	191.252
5	192.096	192.828	190.905
6	191.282	186.508	197.889
7	197.605	190.176	214.873
8	202.847	209.809	201.66
9	193.743	187.795	221.491
10	189.067	186.423	189.859
11	191.068	185.813	188.333
12	193.478	190.219	187.678
13	194.201	190.455	190.517
14	193.848	187.185	196.454
15	195.301	201.83	259.486
16	192.986	204.875	191.468
17	192.167	186.874	221.884
18	197.24	193.865	197.565
19	197.619	196.848	187.81
20	194.885	191.824	220.394
Average	194.2983	193.5703	203.03865
Std dev.	3.126668	7.850288242	17.68421633

(LDV range 125 mm/s/V).

measurement of vibration amplitude is 262.479 mV rms. We used two $\phi 3/32$ in (0.023 g) ceramic balls, and tested the automatic balancing effects when there was thick oil film, thin oil film, and no oil film in the spacer ring. We note here that with thick oil film in the spacer ring, the ball started to move in the spacer ring when the ring was tilted at about 19°. With thin oil film, the balls started to move when the spacer was tilted at 11°. When there is no oil, the ball started to move with a tilt angle of 2°. The tilt angle is thus used as an indicator of friction level in the results given below.

From the experimental results shown in Table 5, although the average vibration amplitude in the case with thin oil film is even lower than that of the case without oil film, it can still be seen that with increased friction in the spacer ring, the standard deviation of the resulting vibration amplitude starts to increase, indicating that the balls are less likely to move to the desired positions and balance the disk/motor pack.

It is worth noting that the oscillatory steady state was also observed during the course of the experiment. The system had a severe vibration after a long time, and the noise caused by the movement of balls was audible. However, with the help of a stroboscope, it was seen that although their self-rotation was very obvious, the balls seemed to move very slowly or stop at

fixed positions, suggesting that the balls had almost the same velocity as the system but different direction.

6. Conclusions

This study presents a precise kinetic model for a commercial optical disk drive with an automatic ball balancing system. First, the vibration characteristics were examined in relation to an unbalance rotating system, and the results obtained served as a basis for analyses carried out later. And then the forces acting on a balancing ball in steady state were formulated. The driving force on the ball was obtained, and the stable and unstable equilibrium positions were identified. Also, the condition to move a ball is ascertained by comparing the driving with frictional forces on it. The equations of motion, with the effects of frictional and driving forces taken into account, were then derived. By employing a commercial software, Matlab, the time responses were subsequently obtained. The statistical results indicate the influence of friction on balls' final dwelling ranges around the desired positions, and consequently, the performance of an ABB. In addition, oscillatory steady state was also discovered in the numerical analyses for the cases with friction only. Finally, experiments are designed and carried out to verify the theoretical analyses, and their results have been found to be in good agreement.

Based on both theoretical and experimental results, it is believed that since an automatic balancing effect is generated by the vibration caused by the imbalance itself, the driving force may be too low to move the balls at low imbalance due to the existence of friction. As such, we could not expect that the imbalance can be reduced indefinitely. Hence, automatic ball balancer may not be suitable for those systems which demand a very low residual imbalance. Reducing the friction or other resistance forces and enlarging the driving force are the two major ways for further reduction of the residual imbalance.

References

[1] P. Bövik, C. Högfors, Autobalancing of rotors, *Journal of Sound and Vibration* 111 (1986) 429–444.
[2] J. Lee, W.K. Van Moorhem, Analytical and experimental analysis of a self-compensating dynamic balancer in rotating mechanism, *ASME Journal of Dynamic Systems, Measurement, and Control* 118 (1996) 468–475.
[3] J. Chung, D.S. Ro, Dynamic analysis of an automatic dynamic balancer for rotating mechanisms, *Journal of Sound and Vibration* 228 (1999) 1035–1056.
[4] J. Chung, I. Jang, Dynamic response and stability analysis of an automatic ball balancer for a flexible rotor, *Journal of Sound and Vibration* 259 (2003) 31–34.
[5] W. Kim, J. Chung, Performance of automatic ball balancers on optical disc drives, *Proceedings of the I MECH E Part C Journal of Mechanical Engineering Science* 216 (2002) 1071–1080.
[6] C. Rajalingham, R.B. Bhat, S. Rakheja, Automatic balancing of flexible vertical rotors using a guided ball, *International Journal of Mechanical Sciences* 40 (1998) 825–834.
[7] C. Rajalingham, S. Rakheja, Whirl suppression in hand-held power tool rotors using guided rolling balancers, *Journal of Sound and Vibration* 217 (1998) 453–466.
[8] W.-Y. Huang, C.-P. Chao, J.-R. Kang, C.-K. Sung, The application of ball-type balancers for radial vibration reduction of the high speed optic disk drives, *Journal of Sound and Vibration* 250 (2002) 415–430.
[9] S.S. Rao, *Mechanical Vibrations*, Addison-Wesley, Reading, MA, 1990.